RSC Advances

PAPER

View Article Online
View Journal | View Issue

Cite this: *RSC Adv.*, 2026, **16**, 25902

Derivatization-assisted dual-mode colorimetric and fluorometric detection of dopamine using 4-hexyl resorcinol

Mohamed N. Goda,[a] Laila S. Alqarni,[a] Faisal K. Algethami,[a] Hossieny Ibrahim,[be] Al-Montaser Bellah H. Ali,[c] Ramadan Ali[d] and Mohamed M. El-Wekil *[cf]

Received 18th March 2026
Accepted 8th May 2026

DOI: 10.1039/d6ra02276f

rsc.li/rsc-advances

The quantification of dopamine (DA) is of great significance because abnormal DA levels are closely linked to several neurological and psychiatric disorders, such as Parkinson's disease, schizophrenia, and depression. In addition, DA analysis plays an important role in clinical diagnosis, pharmaceutical quality assessment, and the investigation of biochemical events in complex biological systems. In this work, a derivatization-based dual-mode sensing strategy was developed for DA determination based on its induced oxidative coupling reaction with 4-hexyl resorcinol (4-HRS) under alkaline conditions. This reaction produces azamonardine, a highly emissive compound that exhibits a strong absorption band at 445 nm and intense fluorescence emission at 490 nm under excitation at 450 nm. The proposed method provided linear responses over the ranges of 0.05–520 μM for colorimetric detection and 10–600 nM for fluorescence detection, with detection limits of 0.018 μM and 3.0 nM, respectively. In addition, the method showed strong sensitivity, acceptable selectivity, mild experimental conditions, and reduced analytical expense. When applied to injection and human serum samples, it produced results consistent with those obtained by LC-MS. Recovery values ranged from 95.0% to 107.2%, and all relative standard deviation (RSD) values were below 3.89%, confirming the method's good accuracy and repeatability.

1. Introduction

Dopamine (DA) is an essential neurotransmitter in the central nervous system, where it regulates motor coordination, behavioral decision-making, and reward-based learning.[1,2] Disturbances in dopaminergic signaling have been linked to several neurological and endocrine disorders, including Tourette syndrome, schizophrenia, pituitary adenomas, and attention deficit hyperactivity disorder.[3,4] Elevated DA levels have been associated with emotional instability, neural damage, irritability, hypertension, and stroke.[5,6] Therefore, the development of reliable analytical methods for DA determination in biological samples is of considerable importance for clinical diagnosis and biomedical research.

A variety of analytical techniques have been employed for DA detection in both *in vitro* and *in vivo* settings, including chromatography,[7] electrochemiluminescence,[8] colorimetry,[9] chemiluminescence,[10] voltammetry,[11] and fluorometry.[12] Among these approaches, optical techniques are particularly attractive because of their high sensitivity, rapid response, and suitability for real-time monitoring.[13–16]

Fluorescence derivatization of DA commonly relies on oxidative coupling reactions that generate highly fluorescent azamonardine derivatives. This strategy has attracted considerable interest owing to its rapid response and high fluorescence quantum yield.[17–19] For example, Dong *et al.* prepared Tb-DPA, Eu-DPA, and Tb/Eu-DPA, which exhibited green, red, and yellow fluorescence, respectively. Based on a "stoplight" signaling strategy, they realized ratiometric fluorescence detection of DA, with the blue emission from the RC–DA reaction serving as the on signal.[18] Ni *et al.* reported an assay for alkaline phosphatase (ALP) in which *p*-nitrophenol, produced through ALP-catalyzed hydrolysis of *p*-nitrophenyl phosphate, effectively quenched the fluorescence of azamonardine.[20]

The induced oxidative coupling of DA with phenolic reagents offers an efficient route for fluorescence derivatization without requiring harsh oxidizing agents, highlighting its strong potential for further analytical applications. In this work, we present a dual-mode colorimetric and fluorescence

[a]*Department of Chemistry, College of Science, Imam Mohammad Ibn Saud Islamic University (IMSIU), Riyadh 11623, Saudi Arabia*
[b]*School of Biotechnology, Badr University in Assiut (BUA), Assiut 2014101, Egypt*
[c]*Department of Pharmaceutical Analytical Chemistry, Faculty of Pharmacy, Assiut University, Assiut, Egypt. E-mail: mohamed.elwakeel@pharm.aun.edu.eg; mohamed.mohamoud@ymail.com*
[d]*Department of Pharmaceutical Chemistry, Faculty of Pharmacy, University of Tabuk, Tabuk 71491, Saudi Arabia*
[e]*Department of Chemistry, Faculty of Science, Assiut University, Assiut 71516, Egypt*
[f]*Pharmaceutical Chemistry Department, Faculty of Pharmacy, Badr University in Assiut (BUA), 2014101 Assiut, Egypt*

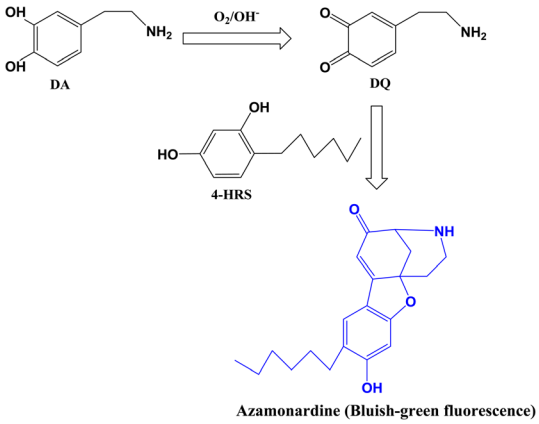

Scheme 1 Proposed pathway for interaction between DA and 4-HRS to form bluish-green fluorescent azamonardine.

derivatization strategy for DA determination based on 4-HRS, and the proposed reaction pathway is illustrated in Scheme 1.

2. Experimental

2.1. Chemicals and instruments

Dopamine hydrochloride (DA), 4-hexyl resorcinol (4-HRS), epinephrine, norepinephrine, 5-hydroxytryptamine, tryptamine, octopamine, uric acid, glucose, lactic acid, glutathione, cysteine, lysine, bovine serum albumin (BSA), glycine, alanine, and ascorbic acid, each with a purity above 98%, were purchased from Sigma-Aldrich (Germany). Sodium dihydrogen phosphate, disodium hydrogen phosphate, hydrochloric acid, sodium hydroxide, and acetonitrile were obtained from Merck. Deionized water was used throughout all experimental measurements and sample preparations.

UV-vis absorption spectra and photoluminescence (PL) measurements were recorded using a Shimadzu UV-1601 PC spectrophotometer and a Shimadzu RF-5301 PC spectrofluorometer, respectively. The pH value was measured at room temperature using a Jenway 3505 digital pH meter (Staffordshire, England). Sonication was performed with an Elmasonic S30 ultrasonic bath (Schmid Bauer GmbH & Co. KG, Singen), while mixing was carried out using a Daihan MSH-20A magnetic stirrer (Korea). Mass spectrometry analysis was carried out in positive ion mode using an LTQ ion-trap mass spectrometer equipped with an electrospray ionization source (Thermo Scientific, USA). H^1-NMR spectrum of azamonardine was acquired on at Agilent solution-state spectrometer after dissolution in DMSO-d_6. Fourier-transform infrared (FT-IR) spectroscopy (Nicolet™ iS™10, Thermo Fisher Scientific, USA) was employed to identify the surface functional groups of the obtained product.

2.2. Detection steps

To quantify DA, 100 μL of 2.5 μM 4-HRS was mixed with 500 μL carbonate buffer at pH 11.0, followed by the addition of 200 μL DA solution of different concentrations. The solution volume was completed to 1.0 mL using deionized water, and the reaction was allowed to proceed for 1 min at 25 °C. The generated product was subsequently measured by colorimetric detection at 445 nm and by fluorescence spectroscopy at λ_{ex} = 450 nm and λ_{em} = 490 nm.

2.3. LC-MS for identification of the reaction product

For product identification, 2.5 mL of 300 μM 4-HRS prepared in deionized water was mixed with 6.2 mL NaOH solution adjusted to pH 11.0 and 1.5 mL of 0.1 mM DA solution. Following 15 min of reaction, the solution was filtered through a 0.22 μm membrane, and the filtrate was analyzed by positive-ion mass spectrometry. Separation by chromatography was conducted employing gradient elution at 0.8 mL min^{-1}, according to the conditions listed in Table S1. An injection volume of 10.0 μL was introduced, while the column temperature remained constant at 30 °C.

2.4. Real samples preparation

The DA injection purchased from a local pharmacy was diluted using 200 μL of the injection and deionized water. Thereafter, a suitable aliquot was withdrawn and subjected to the analytical procedure outlined in Section 2.2.

Serum samples collected from Assiut University Clinics were pretreated by protein precipitation using acetonitrile. Briefly, 1.5 mL of acetonitrile was added to 300 μL of serum, and the mixture was vigorously shaken before centrifugation at 6000 rpm for 20 min. The supernatant was subsequently isolated, filtered through a 0.22 μm membrane, and stored at 4 °C for subsequent use. The study was approved by the Institutional Ethics Committee of Assiut University. Written informed consent was obtained from all participants prior to sample collection. All procedures were performed in accordance with the declaration of Helsinki and applicable national regulations, with participant privacy and safety maintained throughout sample collection, handling, analysis, storage, and disposal.

3. Results and discussions

3.1. Chemical interaction between DA and 4-HRS

The UV/vis absorption and fluorescence characteristics of DA, 4-HRS, and their reaction-derived product were examined at pH 11.0 (Fig. 1). As presented in Fig. 1A, 4-HRS showed nearly no absorbance, while DA exhibited only a weak absorption signal within the 300–500 nm region. In contrast, the reaction product formed between DA and 4-HRS displayed a distinct and intense absorption band with a maximum at 445 nm, indicating the generation of a new chromophoric species after the oxidative coupling reaction. Fluorescence measurements (Fig. 1B) further revealed that both DA and 4-HRS were essentially nonfluorescent under the studied conditions, whereas their interaction product produced a strong emission peak at 490 nm upon excitation at 450 nm. This remarkable optical change confirms the formation of a new fluorescent derivative and highlights the high sensitivity of the reaction system. The emergence of both absorbance and fluorescence responses demonstrates the successful conversion of DA into an optically active product,

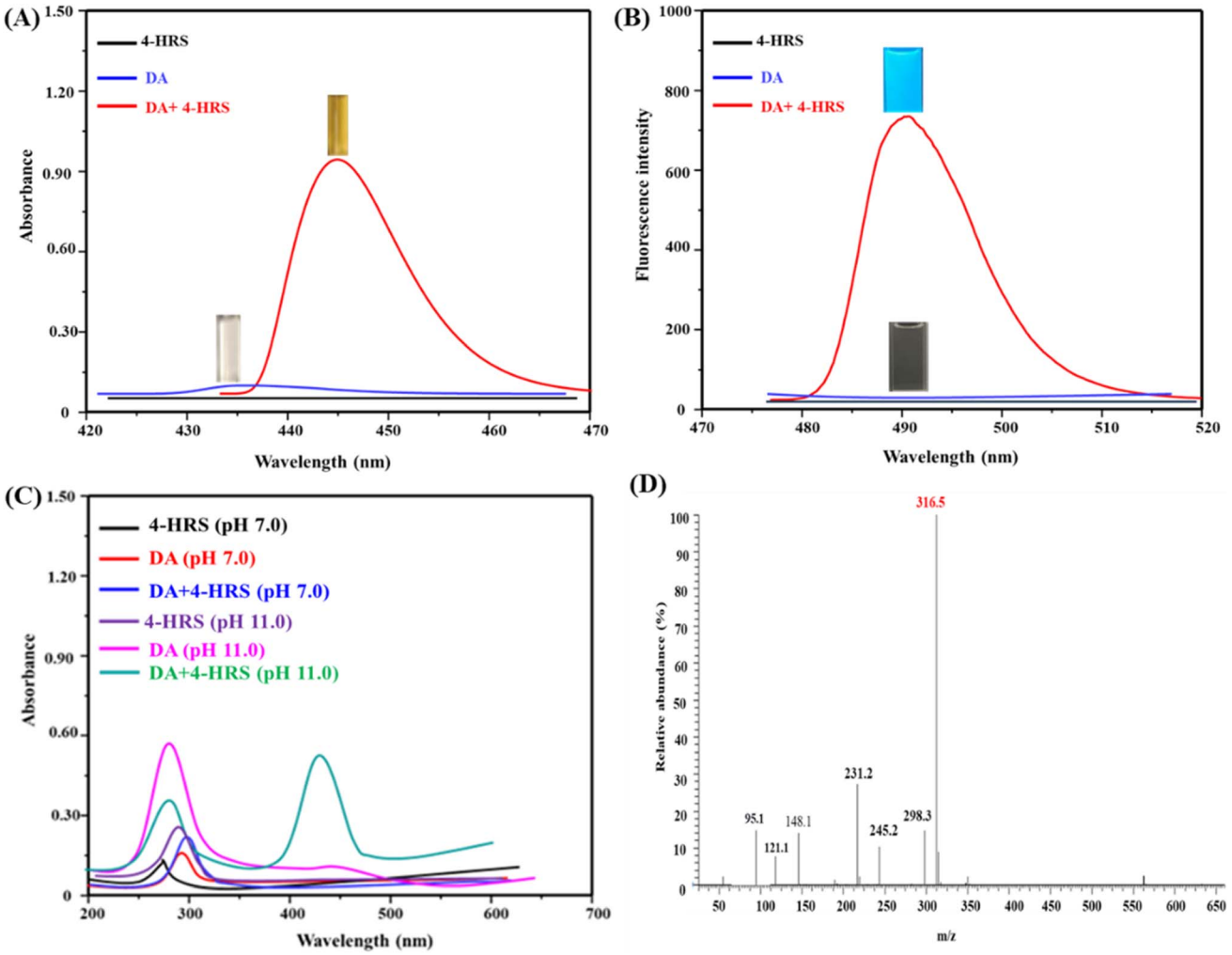

Fig. 1 Absorption (A) and emission (B) spectra of DA+ 4-HRS solution before and after derivatization. (C) Absorption spectra of 4-HRS, DA, and DA+ 4-HRS at pH 7.0 and 11.0. (D) LC-MS of the interaction product of DA and 4-HRS.

thereby providing a reliable basis for its selective colorimetric and fluorometric determination. In comparison with neutral conditions, DA exhibited substantially stronger absorption in alkaline medium (Fig. 1C), suggesting a pronounced change in molecular and electronic structure. At pH 11.0, the phenolic hydroxyl group of DA (pKa ≈ 9.2) becomes deprotonated, which facilitates its oxidation to DA quinone (DQ). This oxidized intermediate is highly reactive and can further undergo derivatization with 4-HRS, producing a strongly fluorescent compound. Therefore, the alkaline environment plays a dual role by promoting DA oxidation and enabling the formation of an optically active derivative suitable for sensitive fluorescence detection.

A plausible mechanism for the fluorescence derivatization reaction is presented in Scheme 1. In alkaline medium, DA is readily oxidized to quinone intermediates because of its catechol moiety. In contrast, 4-HRS, owing to its resorcinol framework, preferentially forms resonance-stabilized monoanionic species rather than being directly oxidized to a quinone species.[21] Subsequently, the oxygen anion derived from 4-HRS can nucleophilically attack the quinone ring of oxidized DA, thereby producing a tricyclic intermediate incorporating a five-membered oxygen-containing heterocycle. This intermediate subsequently undergoes intramolecular nucleophilic addition by either the hydroxyl or amino group of DA quinone to the carbonyl functionality, ultimately yielding the highly fluorescent azamonardine derivative.[22] The pronounced fluorescence enhancement is attributed to the formation of this rigid and extensively conjugated structure, whose extended π-conjugation also promotes stronger light absorption. The proposed structure was further supported by LC-MS analysis, and the suggested reaction pathway was found to be consistent with previously reported studies. As shown in Fig. 1D, the most intense signal appeared at m/z 316.5, which can reasonably be assigned to the protonated molecular ion [azamonardine + H]$^+$ formed through the coupling reaction between DA quinone and 4-HRS. This value is in close agreement with the theoretical m/z of 316.4. The loss of 18 Da (m/z 298.3) corresponds to elimination of a water molecule from a phenolic OH group. The fragments at m/z 245.2 and 231.2 result from sequential cleavage of the hexyl side chain—first loss of

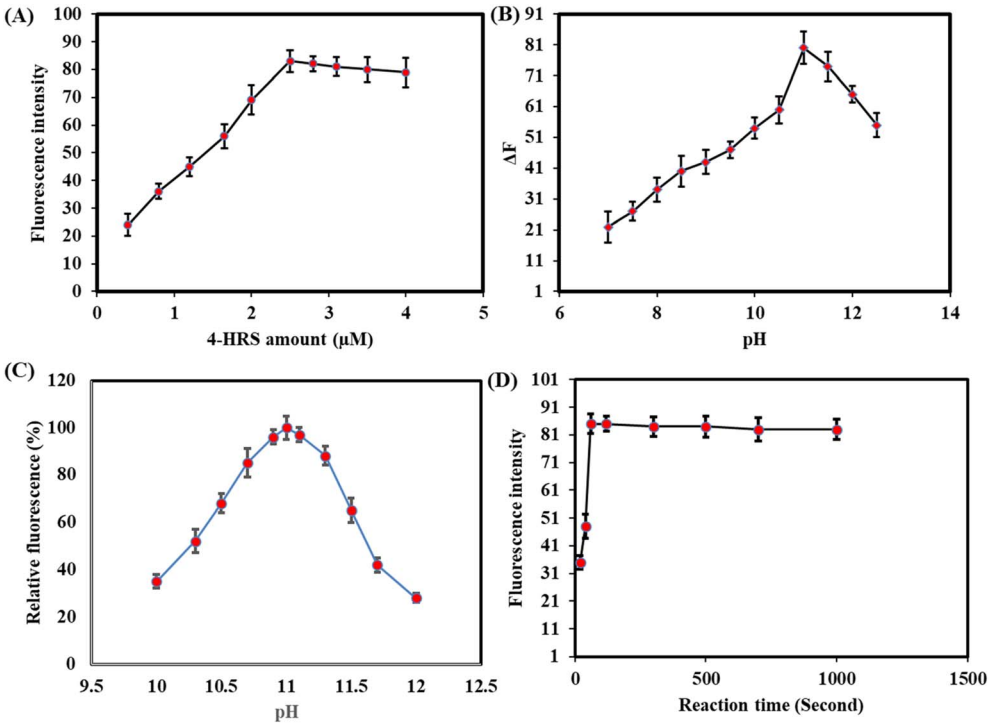

Fig. 2 Effect of (A) 4-HRS amount, (B) pH value, (C) small pH variations (10.0–12.0), and (D) reaction time on the interaction between DA (25.0 nM) and 4-HRS. Number of replicates were five determinations.

C_5H_{11} (71 Da) and then complete loss of C_6H_{13} (85 Da), confirming the presence and length of the alkyl chain. More diagnostically, the fragment at *m*/*z* 148.1 arises from retro-Diels-Alder cleavage of the heterocyclic ring, yielding the DA-derived iminium ion ($C_8H_{10}NO_2^+$). The base peak at *m*/*z* 121.1 corresponds to the protonated catechol fragment ($C_6H_4(OH)_2^+$), while *m*/*z* 95.1 represents the resorcinol-derived fragment ($C_6H_7O^+$). This fragmentation pattern is fully consistent with the proposed tricyclic azamonardine structure and cannot be explained by alternative isomeric products.

Fig. S1A shows the representative chromatogram in which DA and azamonardine were well resolved, with retention times of 8.3 and 10.9 min, respectively. Fig. S1B shows the ^{1}H NMR spectrum (480 MHz, DMSO-d_6) of the purified azamonardine product generated from the reaction of DA with 4-HRS under alkaline conditions (pH 11.0). The spectrum displays characteristic resonances consistent with the proposed azamonardine structure. The broad singlets at δ 9.82 and 8.45 ppm are assigned to the phenolic OH and heterocyclic NH protons, respectively, confirming the presence of exchangeable functional groups. In the aromatic region, signals at δ 7.32 (d, J = 8.4 Hz, 1H), 7.10 (t, J = 8.0 Hz, 1H), and 6.95 (d, J = 8.0 Hz, 1H) are attributed to the aromatic protons of the DA-derived ring, while the resonances at δ 6.48 (s, 1H) and 6.30 (d, J = 2.4 Hz, 1H) are assigned to protons on the resorcinol-derived aromatic ring. The multiplet at δ 2.75–3.30 ppm (4H) corresponds to the DA ethyl bridge (–CH_2–CH_2–N), supporting cyclization and fluorophore formation. In addition, the signals at δ 2.52 (t, J = 7.6 Hz, 2H), 1.55–1.45 (m, 2H), 1.38–1.28 (m, 4H), and 0.88 (t, J = 6.8 Hz, 3H) are assigned to the hexyl substituent of 4-HRS, further confirming its incorporation into the final product. Fig. S1C presents the FT-IR spectrum of the purified azamonardine product, confirming the presence of the main functional groups expected for the target fluorophore. The broad absorption band at 3330 cm^{-1} is assigned to the stretching vibrations of N–H/O–H, indicating the presence of hydrogen-bonded amino and/or hydroxyl groups. The bands in the 2770–2885 cm^{-1} region are attributed to aliphatic C–H stretching vibrations of –CH_2 moieties. A distinct band at 1685 cm^{-1} corresponds to the C=O stretching vibration, supporting the formation of a carbonyl-containing conjugated structure. The absorption at 1555 cm^{-1} can be assigned to N–H/O–H bending and/or conjugated skeletal vibrations, while the band at 1450 cm^{-1} is associated with C=C skeletal vibrations and/or CH_2 bending. In addition, the peaks observed at 1205 and 1108 cm^{-1} are attributed to C–OH/C–O and C–C (or C–O–C) stretching vibrations, respectively. Collectively, these characteristic bands are consistent with the successful formation of azamonardine, and the FT-IR results provide complementary evidence for the proposed molecular structure and purity of the isolated product. In addition, the fluorescence quantum yield of the formed azamonardine was calculated to be 66.8%, using quinine sulfate as the reference standard. These findings collectively confirm the formation of a strongly emissive derivatization product and support the proposed sensing mechanism.

3.2. Optimization of reaction variables

The influence of key experimental parameters on reaction sensitivity was systematically evaluated, as presented in Fig. 2.

The studied factors included 4-HRS concentration, solution pH, and reaction time. As shown in Fig. 2A, the concentration of 4-HRS was varied over the range of 0.4–4.0 μM to determine its effect on fluorescence response. The fluorescence intensity increased progressively with increasing reagent concentration up to 2.5 μM, after which no further improvement was observed. Therefore, 2.5 μM 4-HRS was selected as the optimal concentration and was used throughout the study.

Because both DA and 4-HRS show chemical behavior that varies with pH, the effect of pH on the induced oxidative fluorescence derivatization reaction was systematically investigated (Fig. 2B). The fluorescence signal was relatively weak at neutral and mildly alkaline pH values, but increased markedly as the medium became more alkaline, reaching its maximum at pH 11.0. At pH values below 8.5, the limited deprotonation of the hydroxyl groups in DA likely reduced its susceptibility to oxidation by dissolved oxygen.[23] Under strongly alkaline conditions, DA is more readily converted into semiquinone and quinone intermediates,[24] while 4-HRS can act in its monoanionic form and couple with the quinone species to generate the highly fluorescent azamonardine derivative.[25] At pH values above 11.0, however, the fluorescence intensity decreased, most likely because DA self-polymerization became dominant and competed with the derivatization reaction. Accordingly, pH 11.0 was selected as the optimum buffer condition for subsequent experiments. The effect of small pH variations on the analytical signal was also evaluated to assess method robustness. As shown in Fig. 2C, the fluorescence intensity remained within 95–100% of its maximum value over the narrow pH range of 10.9 to 11.1. Outside this window, the signal decreased rapidly, dropping to 85% at pH 10.7, 88% at pH 11.3, and below 70% at pH values beyond 10.5 or above 11.5. This steep pH dependence arises because the deprotonation of DA (pKa ≈ 9.2) and the subsequent oxidative coupling are highly sensitive to hydroxide ion concentration. Therefore, while pH 11.0 is optimal, careful buffer preparation is essential to maintain pH within ±0.1 unit of the target value to ensure reproducible results.

Reaction time was assessed by recording the fluorescence intensity of the formed product over 1500 s. At the optimized pH of 11.0, the induced oxidative derivatization occurred rapidly after mixing and reached completion within 1 min (Fig. 2D), indicating the fast kinetics of the reaction. Moreover, the generated fluorescent product showed good stability, with no significant change in signal observed for at least 1000 s.

3.3. Analytical merit parameters

The proposed derivatization-assisted dual-mode sensing strategy was successfully applied for DA determination (Fig. 3). As shown in Fig. 3A, the absorbance signal increased progressively with increasing DA concentration over the range of 0.05–520 μM, indicating the formation of the derivatized product. A calibration plot constructed from the change in absorbance (ΔA) *versus* DA concentration exhibited excellent linearity, with the regression equation $\Delta A = 0.0017[\mathrm{DA}] + 0.0816$ and

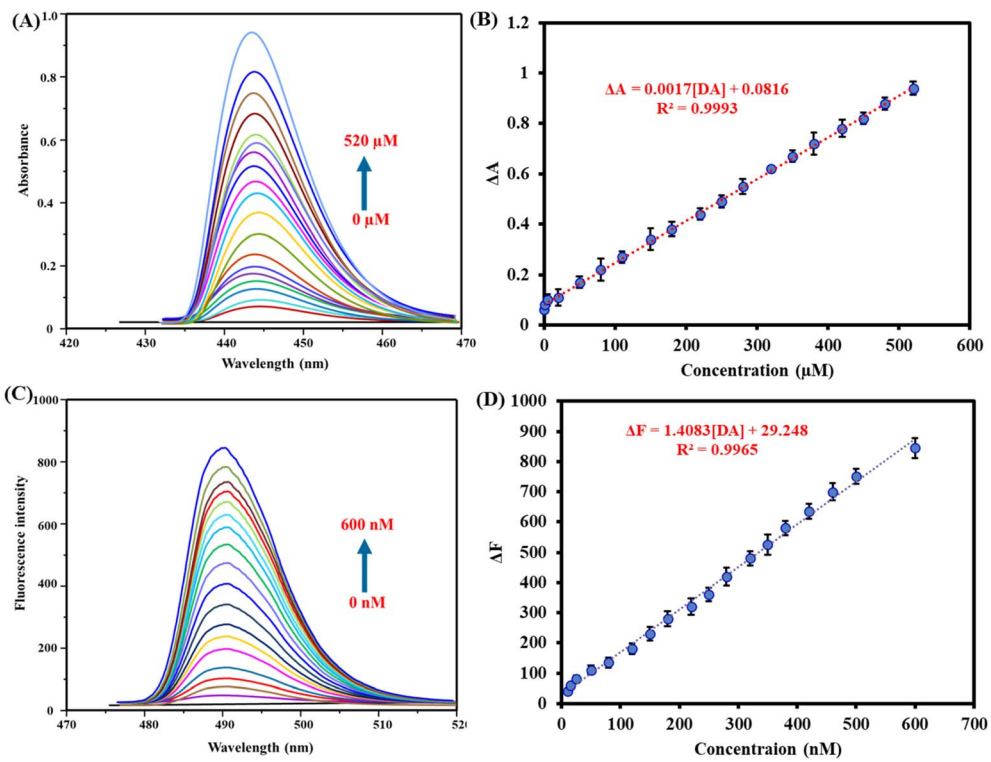

Fig. 3 (A) Absorption spectra of the interaction between DA (0–520 μM) and 4-HRS (2.5 μM); (B) calibration plot between ΔA and concentration of DA; (C) fluorescence spectra of the interaction between DA (0–520 μM) and 4-HRS (2.5 μM); (D) calibration plot between ΔF and concentration of DA. Reaction time is 1 min and pH of phosphate buffer is 11.0. Number of replicates were five determinations.

Table 1 Analytical parameters for determination of DA using the proposed methods

Parameters	Colorimetric	Fluorometric
Linear range (μM)	0.05–520	0.01–0.6
Slope (b)	0.0017	1.408
Standard deviation (SD) of b	5×10^{-5}	0.0048
Intercept (a)	0.0816	29.244
SD of a	9.28×10^{-6}	1.28×10^{-3}
R^2	0.9993	0.9965
LOD (μM)	0.018	0.003
LOQ (μM)	0.05	0.01

a determination coefficient (R^2) of 0.9993 (Fig. 3B). The limit of detection (LOD) for the colorimetric mode was measured according to formula of $3.3\sigma/b$ where σ is standard deviation of intercept and b is slope of calibration plot. The LOD was estimated to be 0.018 μM, confirming the high sensitivity of the method (Table 1). Similarly, the fluorometric response showed a marked enhancement in emission intensity at 490 nm as the DA concentration increased (Fig. 3C). A good linear relationship was observed between the fluorescence difference (ΔF) and DA concentration, following the equation $\Delta F = 1.4083[\mathrm{DA}] + 29.248$, with an R^2 value of 0.9965 (Fig. 3D). The LOD of the fluorescence method was calculated to be 3.0 nM, demonstrating that the fluorometric approach offers even greater sensitivity for DA quantification. Overall, the dual-mode platform provides reliable, sensitive, and complementary detection performance for DA analysis. Table 2 compares the analytical performance of the proposed dual-mode assay with previously reported methods for DA determination. Among these approaches, Dhamra *et al.* reported a sensitive fluorometric assay based on DA derivatization with 1,2-naphthoquinone-4-sulfonate under mildly acidic aqueous conditions at pH 6.0, achieving an LOD of 0.017 μM.[35] Sliesarenko *et al.* developed an *o*-phthalaldehyde-based fluorometric strategy in the presence of pluronic F127, where the micellar environment enhanced the fluorescence response and enabled DA detection with an LOD of 0.015 μM.[36] In a more sophisticated analytical format, Ntorkou *et al.* optimized a pre-column derivatization HPLC-fluorescence method for ultratrace quantification of endogenous DA, attaining a markedly lower LOD of 0.002 μM.[37] These reports demonstrate the effectiveness of derivatization-assisted fluorescence detection for trace DA analysis, particularly when coupled with signal-enhancing media or chromatographic separation to improve sensitivity and selectivity in complex matrices. In comparison, the present dual-mode strategy offers a broad linear working range, low detection limits, and reliable quantitative performance without relying exclusively on chromatographic instrumentation. Therefore, the proposed platform is competitive with existing fluorometric and HPLC-based methods and provides a practical, sensitive, and widely applicable approach for DA determination.

3.4. Precision

To verify the method's reliability, the intra-day and inter-day precision were evaluated, as summarized in Table 3. The relative standard deviation (RSD) values were all below 3.65%, demonstrating the good precision and reproducibility of the derivatization-based colorimetric and fluorometric methods for DA determination.

3.5. Selectivity and reproducibility

The selectivity of the proposed sensing platform toward DA was systematically investigated using a panel of structurally related catecholamines and neurotransmitters commonly encountered in serum, including epinephrine, norepinephrine, 5-hydroxytryptamine, tyramine, and octopamine. As shown in Fig. 4A and B, only DA and, to a lesser extent, epinephrine and norepinephrine, generated appreciable absorbance and fluorescence responses. Importantly, the signal intensity obtained for DA was substantially higher than that of these potential interferents under the optimized assay conditions (pH 11.0, 1 min reaction

Table 2 Comparison of the analytical characteristics of the proposed dual-mode method for DA determination with those of previously reported colorimetric and fluorometric assays

Technique	Probe/reagent	Linear range (μM)	LOD (μM)	Response time (min)	References
Colorimetry	Peroxidase-mimic of N, Fe-CDs	0.05–0.5	0.03	15	26
	Peroxidase-mimic $CoSn(OH)_6$	5–200	4.4	3	27
	Nanofiber/AuNP	0.5–500	0.5	10	28
	Peroxidase-mimic of 3D-MoS_2/graphene	1–400	0.21	10	29
	$CoFe_2O_4$ nanozyme/self-polymerization	5–80	0.233	2.25	30
	BSA-Cu NPs	0.01–60	0.005	20	31
	4-HRS	0–520	0.018	1	This work
Fluorometry	N, Fe-CDs nanozyme	0.10–0.65	0.02	15	26
	BSA-Cu NPs	0.01–10	0.005	20	31
	WS_2 QDs	0–50	3.3	10	32
	NIR-CDs/ARS-3-NPBA	0.1–65	0.035	10	33
	Ag-HA	0.1–70	0.035	20	34
	1,2-Naphthoquinone-4-sulfonic sodium	0.07–13.1	0.017	15	35
	o-Phthalaldehyde/pluronic F127	0.5–3	0.015	80	36
	4-HRS	0–0.6	0.00095	1	This work
Chromatography	Resorcinol (pre-column derivatization)	0.03–65.3	0.002	~10 (separation)	37

Table 3 Interday and intraday precision of the proposed derivatization based dual-mode detection method for DA

		Intraday ($n = 6$)			Interday ($n = 6 \times 3$)		
Technique	Added (μM)	Measured (μM)	Recovery %	RSD %	Measured (μM)	Recovery %	RSD %
Colorimetric	5.0	4.89 ± 0.67	97.8	3.08	4.97 ± 0.84	99.4	1.89
	50.0	53.29 ± 0.56	106.6	3.56	53.56 ± 0.77	107.1	2.78
	100.0	97.88 ± 0.87	106.0	2.67	104.76 ± 0.89	104.8	3.00
Fluorometric	5.0	5.32 ± 0.83	106.4	2.76	5.28 ± 0.87	105.6	2.34
	50.0	47.56 ± 0.43	95.1	2.56	47.80 ± 0.66	95.6	3.56
	100.0	104.53 ± 0.98	104.53	3.01	97.86 ± 0.67	97.9	3.65

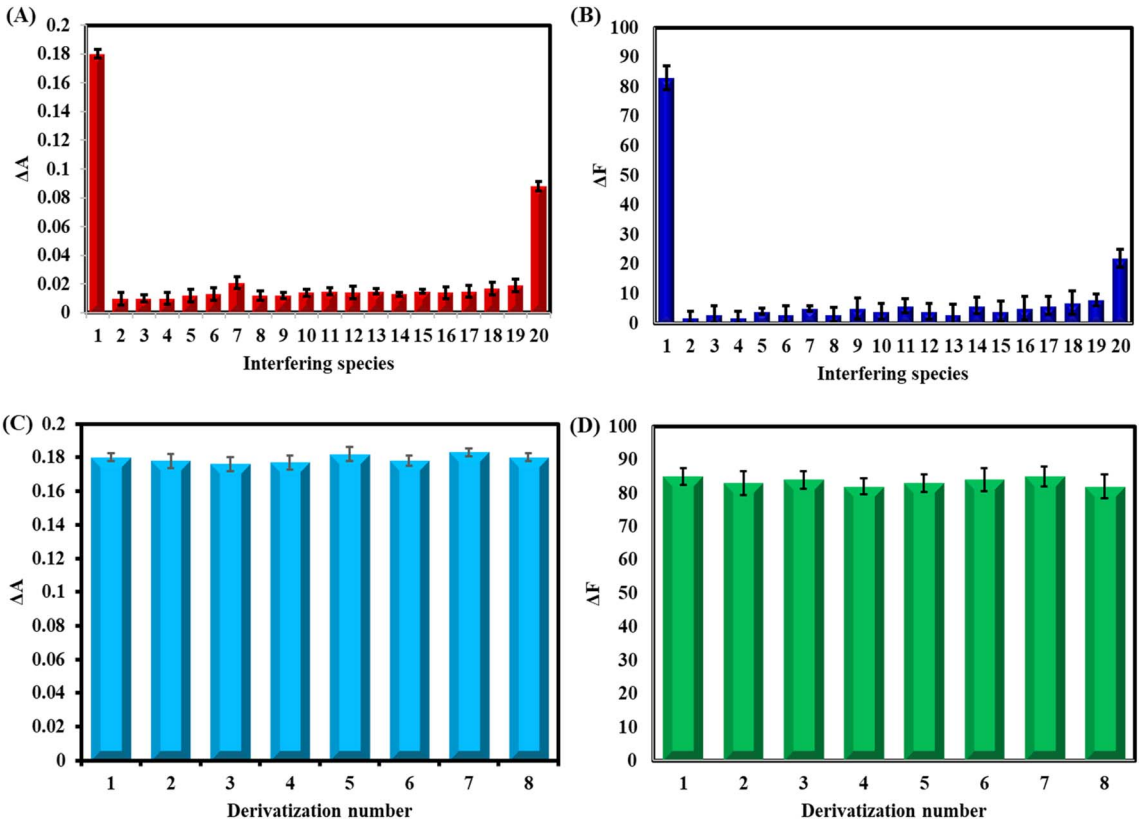

Fig. 4 (A) Colorimetric and (B) fluorometric responses of DA in the presence of 30 folds interfering species (1. DA, 2. Na^+, 3. K^+, 4. Ca^{2+}, 5. Mg^{2+}, 6. uric acid, 7. glucose, 8. lactic acid, 9. glutathione, 10. cysteine, 11. lysine, 12. BSA, 13. glycine, 14. alanine, 15. ascorbic acid, 16. 5-hydroxytryptamine, 17. tryptamine, 18. octopamine, 19. norepinephrine, and 20. epinephrine), DA concentrations used for colorimetric and fluorometric methods were 50 μM and 25 nM, respectively. Other conditions were pH 11.0 and reaction time of 1 min. (C) Colorimetric and (D) fluorometric responses after eight derivatization cycles.

time), highlighting the preferential responsiveness of the method toward the target analyte. In contrast, common serum constituents, including glucose, uric acid, amino acids, and inorganic ions, produced negligible signals, demonstrating excellent anti-interference capability against major endogenous matrix components. Although epinephrine may cause interference when present at unusually high concentrations, this effect can be effectively minimized by appropriate sample dilution or further suppressed through a selective pretreatment/oxidation step. Therefore, for routine determination of DA in serum, particularly in subjects not receiving exogenous epinephrine, the proposed method provides satisfactory selectivity, good analytical reliability, and promising practical applicability in complex biological matrices.

The absorbance and fluorescence responses at the selected wavelengths were recorded following eight independent derivatization runs. The obtained relative standard deviation (RSD) was 2.89%, confirming the good reproducibility of the method (Fig. 4C and D).

3.6. Applications

To further verify the practical applicability of the method, it was employed for the quantification of DA in DA injection and

Table 4 Determination and recovery results of DA in real samples using colorimetric and LC-MS methods ($n = 3$)

		Fluorometric method			LC-MS		
Samples	Added (μM)	Found (μM)	% Recovery	% RSD	Found (μM)	% Recovery	% RSD
Injection	0.0	4.67	—	2.67	5.34	—	3.78
	1.0	5.71	104.0	2.54	6.40	106.0	4.65
	5.0	9.67	100.0	3.43	10.67	106.6	4.02
	10.0	15.12	104.5	2.00	15.76	104.2	4.76
	20.0	24.47	99.0	1.87	26.34	105.0	3.76
Serum	0.0	ND	—	—	ND	—	—
	1.0	1.03	103.0	2.67	1.07	107.0	4.78
	5.0	4.78	95.6	3.09	5.32	106.4	3.90
	10.0	9.87	98.7	2.67	10.84	108.4	4.20
	20.0	21.43	107.2	1.27	19.14	95.7	3.89

Table 5 Determination and recovery results of DA in real samples using fluorometric and LC-MS methods ($n = 3$)

		Fluorometric method			LC-MS		
Samples	Added (μM)	Found (μM)	% Recovery	% RSD	Found (μM)	% Recovery	% RSD
Injection	0.0	0.023	—	3.78	0.027	—	4.77
	0.1	0.120	97.0	3.89	0.123	96.0	4.00
	0.15	0.172	99.3	2.76	0.182	103.3	3.55
	0.20	0.230	103.5	2.66	0.237	105.0	4.88
	0.25	0.265	96.8	4.08	0.278	100.4	3.67
Serum	0.0	ND	—	—	ND	—	—
	0.1	0.104	104.0	3.76	0.107	107.0	4.34
	0.15	0.147	98.0	3.48	0.140	93.3	3.98
	0.20	0.198	99.0	2.00	0.192	96.0	4.77
	0.25	0.258	103.2	3.78	0.257	102.8	3.56

serum samples. Method accuracy was evaluated by comparing the results with those obtained by liquid chromatography and by performing spike-recovery experiments at various DA concentrations. Each sample was analyzed in triplicate. As summarized in Tables 4 and 5, the measured values showed good agreement with the liquid chromatography data. The recoveries fell within 95.0–107.2%, and all RSD values were below 3.89%, indicating excellent accuracy and good repeatability. Overall, these results confirm that the proposed method is reliable for quantitative DA determination in real matrices.

4. Conclusions

In summary, a derivatization-based dual-mode analytical method was successfully established for DA detection. When exposed to alkaline conditions, DA participates in an induced oxidative coupling reaction with 4-HRS, yielding azamonardine as a strongly fluorescent product. Owing to its high sensitivity, acceptable selectivity, and low cost, the proposed method is attractive for routine analytical applications. A good linear relationship was observed between azamonardine's colorimetric response and DA concentration over the range of 0.05–520 μM, yielding a detection limit of 0.018 μM. Moreover, the fluorescence response exhibited excellent linearity over 10–600 μM, with a lower detection limit of 3.0 nM. In contrast to photocatalytic oxidative derivatization methods, this approach does not require any catalyst and is less affected by fluctuations in light intensity, which improves its practicality and robustness. UV-vis and LC-MS results further supported the reaction mechanism, indicating that DA is initially oxidized to DA quinone (DQ), followed by nucleophilic coupling of monoanionic 4-HRS with DQ to produce azamonardine.

Conflicts of interest

The authors declare no competing interests.

Data availability

Data will be available upon request from the corresponding author.

Supplementary information (SI) is available. See DOI: https://doi.org/10.1039/d6ra02276f.

Acknowledgements

This work was supported and funded by the Deanship of Scientific Research at Imam Mohammad Ibn Saud Islamic University (IMSIU) (grant number IMSIU-DDRSP2601).

References

1 S. J. Lee, B. Lodder, Y. Chen, T. Patriarchi, L. Tian and B. L. Sabatini, Cell-type-specific asynchronous modulation of PKA by dopamine in learning, *Nature*, 2020, **590**(7846), 451–456.

2 P. Kosillo, N. M. Doig, K. M. Ahmed, A. H. C. W. Agopyan-Miu, C. D. Wong, L. Conyers, S. Threlfell, P. J. Magill and H. S. Bateup, Tsc1-mTORC1 signaling controls striatal dopamine release and cognitive flexibility, *Nat. Commun.*, 2019, **10**(1), 5426.

3 D. Vallone, R. Picetti and E. Borrelli, Structure and function of dopamine receptors, *Neurosci. Biobehav. Rev.*, 2000, **24**, 125–132.

4 A. M. Mahmoud, M. H. Mahnashi, K. Alhazzani, A. Z. Alanazi, M. M. Algahtani, A. Alaseem, B. A. Alyami, A. O. AlQarni and M. M. El-Wekil, Nitrogen doped graphene quantum dots based on host guest interaction for selective dual readout of dopamine, *Spectrochim. Acta, Part A*, 2021, **252**, 119516.

5 M. Y. Malik, F. Guo, A. A. Malik, V. Eftychidis, K. N. Timm, A. Wolska, D. Bergin, B. Zonta, V. R. Wirsching, S. V. Hörsten, M. E. Walton, P. J. Magill, C. Nerlov and L. Minichiello, Impaired striatal glutathione–ascorbate metabolism induces transient dopamine increase and motor dysfunction, *Nat. Metab.*, 2024, **6**(11), 2100–2117.

6 Y. Chen, Y. H. Gu, B. B. Wang, A. Q. Wei, N. Dong, X. Y. Liu, L. Zhu, F. Zhu, Y. Jiang, F. H. Mao, Y. C. Zhang, J. Y. Yao, T. Tan, Z. X. Jing, Y. X. Yang, H. Y. Wang, H. Wu, H. Li, C. W. Zheng, X. T. Duan, J. X. Huo, X. A. Wu, S. Q. Hu, A. R. Zhao, Z. Y. Li, X. Cheng, Y. H. Qin, Q. Song, S. Q. Zhan, Q. M. Qu, F. L. Guan, X. J. Kang and C. H. Wang, Synaptotagmin-11 deficiency mediates schizophrenia-like behaviors in mice via dopamine over-transmission, *Nat. Commun.*, 2024, **15**(1), 10571.

7 F. C. Chen, B. X. Fang, P. Li and S. C. Wang, A fast and validated HPLC method for the simultaneous analysis of five 5-HT3 receptor antagonists via the quantitative analysis of multicomponents by a single marker, *Int. J. Anal. Chem.*, 2021, 1–9.

8 F. Li, H. Peng, N. T. Shen, C. Yang, L. M. Zhang, B. Li and J. B. He, Electrochemiluminescence in graphitic carbon nitride decorated with silver nanoparticles for dopamine determination using machine learning, *ACS Appl. Mater. Interfaces*, 2024, **16**(21), 27767–27777.

9 P. Sun, M. Z. Shang, F. Zhang and F. Chai, Dual-mode fluorimetric and colorimetric sensors based on iron and nitrogen co-doped carbon dots for the detection of dopamine, *Food Chem.*, 2024, **445**, 138794.

10 R. Afsharipour, S. Dadfarnia and A. M. H. Shabani, Chemiluminescence determination of dopamine using N, P-graphene quantum dots after preconcentration on magnetic oxidized nanocellulose modified with graphene quantum dots, *Microchim. Acta*, 2022, **189**, 192.

11 S. A. Alkahtani, A. M. Mahmoud, R. Ali and M. M. El-Wekil, Sonochemical synthesis of lanthanum ferrite nanoparticle–decorated carbon nanotubes for simultaneous electrochemical determination of acetaminophen and dopamine, *Microchim. Acta*, 2024, **191**, 25.

12 C. H. Liu, X. F. Lin, J. Liao, M. Yang, M. Jiang, Y. Huang, Z. Z. Du, L. N. Chen, S. J. Fan and Q. T. Huang, Carbon dots-based dopamine sensors: recent advances and challenges, *Chin. Chem. Lett.*, 2024, **35**(12), 109598.

13 B. A. Alyami, A. M. Mahmoud, A. O. Alqarni and M. M. El-Wekil, Intrinsic self-calibration electrostatic-controlled ratiometric fluorescence assay of histamine in human serum and canned tuna fish samples, *Microchem. J.*, 2023, **195**, 109388.

14 R. Ali, A. H. Alharbi, M. H. Alatwi, F. M. Albalawi, E. M. Albalawi, A. H. Alahmadi, N. M. Alanazi, A. M. Humadi, A. Z. A. Albalawi and M. M. El-Wekil, Colorimetric detection of kasugamycin via silver oxide nanoparticles with intrinsic laccase activity, *Food Chem.*, 2026, **508**, 148063.

15 Y. A. Bin Jardan, M. M. El-Wekil, M. R. Elmasry and A. B. H. Ali, Dual emissive nanoprobe for reliable detection of antipsychotic drug fluphenazine using silicon nanoparticles and eosin dye, *J. Photochem. Photobiol., A*, 2025, **468**, 116464.

16 Y. A. Bin Jardan, A. M. Mostafa, J. Barker, A. B. H. Ali and M. M. El-Wekil, A novel route for fabrication of yellow emissive carbon dots for selective and sensitive detection of vitamin B12, *Anal. Methods*, 2025, **17**, 3007–3016.

17 J. Zhao, X. Bao, S. Wang, S. Lu, J. Sun and X. Yang, In situ fluorogenic and chromogenic reactions for the sensitive dual-readout assay of tyrosinase activity, *Anal. Chem.*, 2017, **89**, 10529–10536.

18 X. Z. Dong, Z. Sun, L. Han, Y. Ling, B. L. Li, N. B. Li and H. Q. Luo, A "traffic light" signal ratiometric fluorescence sensor for highly sensitive and selective detection of dopamine, *Sens. Actuators, B*, 2022, **372**, 132668.

19 J. Zhang, D. Xu, Y. Zhang, Z. Luo, Y. Zhao, X. Zheng, H. Yang and Y. Zhou, Gold nanoparticle-mediated fluorescence immunoassay for rapid and sensitive detection of Ochratoxin A, *Spectrochim. Acta, Part A*, 2024, **304**, 123312.

20 P. Ni, C. Chen, Y. Jiang, C. Zhang, B. Wang, Y. Lu and H. Wang, A fluorescent assay for alkaline phosphatase activity based on inner filter effect by in-situ formation of fluorescent azamonardine, *Sens. Actuators, B*, 2020, **302**, 127145.

21 E. G. F. de Miranda, L. M. Cornetta and M. T. do N. Varella, Low-energy electron interactions with resveratrol and resorcinol: anion states and likely dissociation pathways, *J. Phys. Chem. A*, 2022, **126**, 7667–7674.

22 A. U. Acuña, F. Amat-Guerri, P. Morcillo, M. Liras and B. Rodríguez, Structure and formation of the fluorescent compound of lignum nephriticum, *Org. Lett.*, 2009, **11**, 3020–3023.

23 T. Long, J. Cheng, C. Peng, W. Xu, H. Luo, M. Ouyang, D. Xu, Q. Lin, J. Qu and X. Huang, Highly sensitive and rapid detection of resorcinol by forming fluorescent azamonardine with dopamine, *Anal. Biochem.*, 2022, **642**, 114562.

24 W. Chan, Investigation of the chemical structure and formation mechanism of polydopamine from self-assembly of dopamine by liquid chromatography/mass spectrometry coupled with isotope-labelling techniques, *Rapid Commun. Mass Spectrom.*, 2019, **33**, 429–436.

25 M. Iacomino, M. L. Alfieri, O. Crescenzi, M. d'Ischia and A. Napolitano, Unimolecular variant of the fluorescence turn-on oxidative coupling of catecholamines with resorcinols, *ACS Omega*, 2019, **4**, 1541–1548.

26 B. Wang, Y. Chen, Y. Wu, B. Weng, Y. Liu and C. M. Li, Synthesis of nitrogen- and iron-containing carbon dots, and their application to colorimetric and fluorometric determination of dopamine, *Microchim. Acta*, 2016, **183**, 2491–2500.

27 H. Liu, Y.-N. Ding, B. Bian, L. Li, R. Li, X. Zhang, Z. Liu, X. Zhang, G. Fan and Q. Liu, Rapid colorimetric determination of dopamine based on the inhibition of the peroxidase mimicking activity of platinum loaded $CoSn(OH)_6$ nanocubes, *Microchim. Acta*, 2019, **186**, 755.

28 A. Rostami, A. Hadjizadeh and S. Mahshid, Colorimetric determination of dopamine using an electrospun nanofibrous membrane decorated with gold nanoparticles, *J. Mater. Sci.*, 2020, **55**, 7969–7980.

29 Q. Lv, L.-s. Chen, H.-x. Liu and L.-l. Zou, Peony-like 3D-MoS2/graphene nanostructures with enhanced mimic peroxidase performance for colorimetric determination of dopamine, *Talanta*, 2022, **247**, 123553.

30 P. Sun, J. Chen, Q. Li, M. Luo, W. Chang and Z. Xue, Self-signaling colorimetric sensor for selective detection of dopamine based on $CoFe_2O_4$ nanozyme accelerated dopamine polymerization, *Anal. Chim. Acta*, 2025, **1338**, 343596.

31 D.-Q. Feng, S. Wang, Z. Yu, W. Zhang and G. Liu, Dual-recognition driven sensing platform based on a BSA-Cu NP nanozyme combined with smartphone-assistance for fluorometric/colorimetric monitoring of dopamine, *RSC Adv.*, 2025, **15**, 199–206.

32 L. Haghighi, N. Haghnazari and C. Karami, Tungsten disulfide quantum dots (WS_2 QDs) as a fluorescence probe for detection of dopamine (DA), *J. Mater. Sci.:Mater. Electron.*, 2021, **32**, 28042–28050.

33 G. Alasiri, A. M. Alaseem, M. M. El-Wekil, R. Ali and A. B. H. Ali, Ratiometric detection of dopamine using NIR carbon dots and Alizarin red S-boronic acid complex: A competitive displacement approach, *Spectrochim. Acta, Part A*, 2026, **348**, 127251.

34 Y. Chen, C. Zhou, W. Zhang, H. Wang and X. Su, Bifunctional fluorescent silver-based peroxidase-mimetic nanozymes: A novel ratiometric fluorescence/colorimetric dual-signal system for dopamine detection, *Talanta*, 2026, **300**, 129167.

35 M. Y. Dhamra, T. N. Al-Sabha and M. Al-Enizzi, Spectrofluorimetric determination of adrenaline and dopamine, *J. Educ. Sci.*, 2022, **31**(3), 17–26.

36 V. Sliesarenko, U. Bren and A. Lobnik, Fluorescence based dopamine detection, *Sens. Actuators Rep.*, 2024, **7**, 100199.

37 M. Ntorkou, P. D. Tzanavaras and C. K. Zacharis, Ultrasensitive detection of neurotransmitter dopamine in human urine via fluorescent azamonardine formed with resorcinol, *J. Chromatogr. A*, 2026, **1767**, 466633.